Particle acceleration by breaking of the constrictions of a Z-pinch and a plasma focus

B. A. Trubnikov and S. K. Zhdanov

I. V. Kurchatov Institute of Atomic Energy
(Submitted July 14, 1975)
Zh. Eksp. Teor. Fiz. **70**, 92–103 (January 1976)

It is demonstrated that the condition $E > B$ may be reached during the course of the development of instabilities of the constriction type in the plasma column of a discharge. In this case the particle motion ceases being of the drift type and "direct" particle acceleration in an electric field E_z becomes possible.

PACS numbers: 52.55.Ez, 52.35.En, 52.80.−s

1. It is well known[1] that particles accelerated to energies ~300 keV and higher are observed in high-power pulsed discharges with currents $J \sim 200$–1000 kA. In discharges in deuterium, these particles—deuterium ions—give rise to a certain number of nuclear reactions accompanied by emission of neutrons, as many as $\sim 10^8$ in Z pinches,[2] 10^9–10^{11} in a plasma focus,[3] and up to 10^{12} in coaxial "guns."[4] One of us[5] has advanced the hypothesis that the abrupt narrowing of the cross section in the constrictions leads to a blocking of the conduction current, which is replaced in part by the displacement current

$$j_{dis} = \frac{1}{4\pi}\frac{\partial \varepsilon E}{\partial t}.$$

This should lead to an increase of the field E_z, which can cause a repeated breakdown on the periphery of the discharge and to accelerate a certain fraction of the particles. An objection against this mechanism may be the argument that acceleration across the magnetic field is impossible, especially for electrons. However, if the electric field E exceeds the magnetic field B, then the particle motion is no longer of the drift type and the acceleration becomes possible. In this paper we investigate this possibility by using a number of model examples.

2. The model problem of the breaking of the constriction was investigated by one of us[6] on the basis of the cylindrical wave equation[1)]

$$\Box E_z = \frac{\partial}{r\,\partial r} r \frac{\partial E}{\partial r} - \frac{\partial^2 E}{c^2\,\partial t^2} = 0, \tag{1}$$

the simplest solution of which is a wave of the type (see Fig. 1)

$$E = 2J_0/c(c^2t^2 - r^2)^{1/2}, \tag{2}$$

which is produced when an infinitesimally thin wire with current J_0 is suddenly broken. It appears that such a case was apparently observed in coaxial guns (see Fig. 2).

In many cases, however, the break is not instantaneous (see Fig. 3). In addition, the medium surrounding the pinch is not always a vacuum, since the entrapment of the plasma in the contracting discharge is not complete. These two important circumstances can be taken into account in the following manner. Assume that the breaking of the current proceeds in steps—first at $t = 0$ the current decreases by δJ_0, then at $t = t_1$ by δJ_1, etc. Then at a radius $r < ct$ we obtain a sum of waves of the type (2), which manage to reach the indicated distance. We thus obtain a field in the form

$$E(r,t) = \sum_{i=0}^{\max} \frac{2\delta J_i}{c[c^2(t-t_i)^2 - r^2]^{1/2}} = \frac{2}{c}\int_0^{t-r/c} \frac{-J_0(t')\,dt'}{[c^2(t-t')^2 - r^2]^{1/2}}, \tag{3}$$

where $J_0(t)$ is the derivative of the current with respect to time. For example, for currents that decrease linearly and parabolically we obtain (at $t < T$)

$$E = \frac{2J_0}{c^2 T}\operatorname{Arch}\frac{1}{\rho} \quad \text{at} \quad J_0(t) = J_0\left(1 - \frac{t}{T}\right),$$
$$E = \frac{4J_0 t}{c^2 T^2}\left[\operatorname{Arch}\frac{1}{\rho} - (1-\rho^2)^{1/2}\right] \quad \text{at} \quad J_0(t) = J_0\left(1 - \frac{t^2}{T^2}\right), \tag{4}$$

where

$$\rho = r/ct < 1.$$

The front of these waves propagates with the speed of light, but if account is taken of the influence of the residual plasma in the space surrounding the pinch, then the situation changes. The wave should propagate in this case with Alfven velocity and it is therefore necessary to make in (1) the substitution $c \to c_A = B/(4\pi M n_{extr})^{1/2}$.

Experimental data on the density of the residual plasma which is not trapped in the pinch are scanty. According to Gribkov's estimates[8] its density is smaller by three or four orders of magnitude than the density of the plasma in the pinch ($n_{pinch} \sim 10^{17}$–10^{18} cm^{-3} in Z pinches and 10^{18}–10^{19} cm^{-3} in plasma-focus installations). It is reasonable to assume that at the chamber walls $r = R_W$ this density is equal to the initial density of the gas $n_0 \sim 4 \cdot 10^{16}$ cm^{-3} (at an initial pressure ~1 mm Hg), and then falls off towards the axis in accordance with some law, say linear: $n_{extr} = rn_0/R_W$. Photographs of discharges, taken "from the end," show[9] that the contracting sheath is not strictly cylindrical, but has a a noticeable string-net structure, so that the assumption that not all of the plasma gets trapped in the pinch

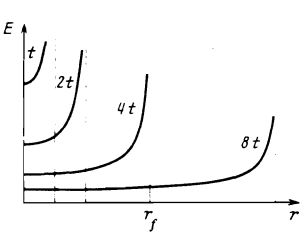

FIG. 1. Profile of the field $E(r,t)$ of the wave (2) at different instants of time.

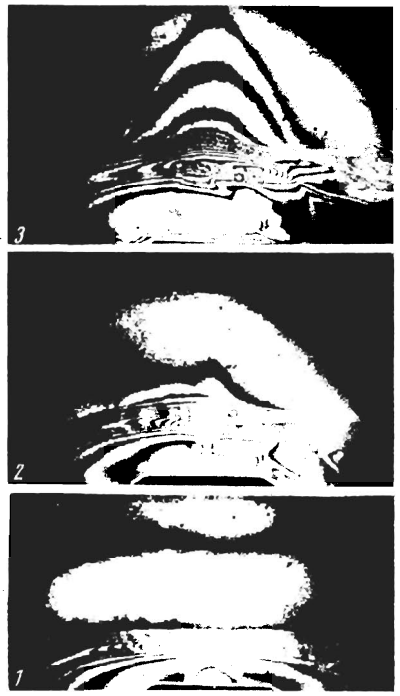

FIG. 2. Three successive photographs of a pinch. The start of the neutron emission coincides with the instant when a visible complete break of the pinch appears on photograph 2.

is quite acceptable.

Typical values of the chamber radius and of the current at the instant of the "second singularity," which coincides with the start of the neutron radiation,[10] are $R = 10$ cm and $J = 200$ kA for a Z pinch and $R = 50$ cm and $J = 1$ MA for a plasma focus. The Alfven velocity c_A^w at the wall is in this case $\varkappa = c_A^w/c = 2J/c^2R(4\pi Mn_0)^{1/2} \sim 10^{-4}$ times smaller than the speed of light. Recognizing that $B \sim 1/r$ and assuming $n_{\text{extr}} \sim r$, we obtain $c_A(r) = (R/r)^s c_A^w$, where $s = \frac{3}{2}$. Making the substitution $c \to c_A(r)$, we rewrite (1) in the form

$$\Delta E - \frac{1}{c_A^2}\frac{\partial^2 E}{\partial t^2} = \frac{\partial}{r\,\partial r} r \frac{\partial E}{\partial r} - \frac{(r/R)^{2s}}{\varkappa^2 c^2}\frac{\partial^2 E}{\partial t^2} = 0. \qquad (5)$$

The front of wave propagates now in accordance with the law

$$dr_f/dt = c_A(r_f) = \varkappa c (R/r_f)^s,$$

whence

$$r_f(t) = R[\varkappa(s+1)ct/R]^{1/(s+1)}.$$

At $s = \frac{3}{2}$ and $\varkappa = 10^{-4}$, the wave reaches the wall of the chamber within the time $t_w = 1300$ nsec in a Z pinch with $R = 10$ cm, and within a time $t_w = 6000$ nsec in a plasma focus with $R = 50$ cm, whereas in vacuum this time would be $R/c \sim 1$ nsec.

Thus, allowance for the presence of the surrounding plasma alters significantly the temporal characteristics of the constriction-breaking process. If instead of r we introduce a new variable

$$x = R(r/R)^{s+1}/\varkappa(s+1),$$

then Eq. (5) takes the form

$$\varkappa^2\left(\frac{R}{r}\right)^{2s}\frac{\partial}{r\,\partial r} r \frac{\partial E}{\partial r} - \frac{\partial^2 E}{c^2\,\partial t^2} = \frac{\partial}{x\,\partial x} x \frac{\partial E}{\partial x} - \frac{\partial^2 E}{c^2\,\partial t^2} = 0, \qquad (6)$$

which coincides formally with Eq. (1). The electric and magnetic field are best expressed in terms of the vector potential $\bar{A}$ of the wave:

$$E = -\frac{\partial \bar{A}}{c\,\partial t}, \quad B = \frac{2J_0(0)}{cr} + \bar{B}, \quad \bar{B} = -\frac{\partial \bar{A}}{\partial r}, \qquad (7)$$

which also satisfies Eq. (6).

The introduction of the vector potential $\bar{A}$ is convenient because the plasma pinch can henceforth be regarded as ideally conducting, and one can assume that at its boundary $r = a(t)$ there is satisfied the condition $E = -vB/c$, which reduces to the equation

$$E|_{r=a} = -\left(\frac{\partial \bar{A}}{c\,\partial t}\right)_{r=a} = -\frac{\dot{a}}{c}\left[\frac{2J_0(0)}{ca(t)} - \left(\frac{\partial \bar{A}}{\partial r}\right)_{r=a}\right]. \qquad (8)$$

From this we get

$$\bar{A}(t, r=a(t)) = \left(\frac{2J_0(0)}{c}\right)\ln\frac{a(t)}{a_1},$$

which in fact determines the motion of the sheath of the pinch. The constant a_1 is obtained from the initial conditions. With this formulation of the problem, the current $J_0(t)$ on the axis is in essence a fictitious auxiliary quantity, whereas the real current $J(t)$ flowing through the constriction is determined from the relation $J(t) = 1/2ca(t)B(t, r = a(t))$.

The solutions corresponding to a gradual breaking of an infinitesimally thin current $J_0(t)$ on the axis take the form (at $x < ct$)

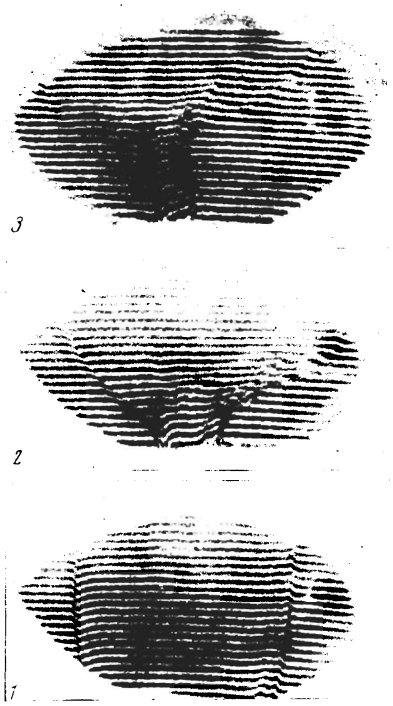

FIG. 3. Three successive photographs of a plasma focus with long-lived residual constrictions.

$$B=\frac{2}{cr}\left\{J_0(0)+\int_0^{t-x/c}\left[(t-t')^2-\left(\frac{x}{c}\right)^2\right]^{-1/2}(t-t')J_0(t')\,dt'\right\}.$$

$$E=-\frac{2}{(s+1)c^2}\int_0^{t-x/c}\left[(t-t')^2-\left(\frac{x}{c}\right)^2\right]^{-1/2}J_0(t')\,dt',$$

$$\bar{A}=-\frac{2J_0(0)}{c(s+1)}\operatorname{Arch}\frac{ct}{x}+\frac{2}{c(s+1)}\int_0^{t-x/c}\left[(t-t')^2-\left(\frac{x}{c}\right)^2\right]^{-1/2}J_0(t')\,dt'. \tag{9}$$

It can also be shown that the waves diverging from the axis and having a front $x_{1f}=ct$ are described in the general case by a series of the type

$$\bar{A}=\sum_n a_n y^n Q_n(z),\quad z=\left[1-\left(\frac{x}{ct}\right)^2\right]^{-1/2},\quad y=\frac{t}{z}$$

where $Q_n(z)$ is a Legendre function of the second kind. Thus, the formulation proposed here for the problem, in contrast to that assumed earlier,[6] takes three factors into account: a gradual rather than instantaneous character of the interruption of the current, the presence of a plasma surrounding the pinch, and a transition to a boundary-value problem with the condition $E=-vB/c$ on the surface of the pinch.

3. We now take into account a fourth and apparently most important circumstance, namely: we assume that the current in the constriction is not "completely" interrupted, and show that under these conditions the "$E>B$" situation, which makes particle acceleration possible, sets in for the considered model of the contracting pinch in a regular manner, and is inevitable.

In fact, when the fictitious current on the axis is instantaneously decreased from the value J_0 to $J_0-J_1>0$, we have (cf. (2))

$$\bar{A}=-\frac{2J_1}{c(s+1)}\operatorname{Arch}\frac{ct}{x},\quad \bar{E}=\frac{2J_1/c(s+1)}{(c^2t^2-x^2)^{1/2}},\quad \bar{B}=-\frac{2J_1/cr}{[1-(x/ct)^2]^{1/2}}. \tag{10}$$

On the front $x=ct$ we have here $\bar{E}=+\infty$ and $\bar{B}=-\infty$ (!), and this case is difficult to compare with experiment, but it is easy to foresee that at a certain sufficiently small smearing of the front of this wave one can obtain finite values of E and B, but then B can still remain, in a certain section, a negative quantity exceeding in absolute magnitude the main field $B_0=2J_0/cr$.

Let us explain this important circumstance using a very simple example with a linear decrease of the fictitious current

$$\begin{aligned} &J_0(t)=J_0-J_1t/T \quad \text{if} \quad t<T,\\ &J_0(t)=J_0-J_1>0 \quad \text{if} \quad t>T. \end{aligned} \tag{11}$$

Substituting these expressions in the first formula of (9) for the total magnetic field, we obtain

$$B=\frac{2}{cr}\left\{J_0-\frac{J_1}{T}\left[t^2-\left(\frac{x}{c}\right)^2\right]^{1/2}\right\},\quad c(t-T)<x<ct;$$

$$B=\frac{2}{cr}\left\{J_0-\frac{J_1}{T}\left[\left(t^2-\left(\frac{x}{c}\right)^2\right)^{1/2}-\left((t-T)^2-\left(\frac{x}{c}\right)^2\right)^{1/2}\right]\right\},\quad x<c(t-T). \tag{12}$$

In contrast to the case (10), the field (12) does not become infinite anywhere, and on the leading front $x_{1f}=ct$ it is equal to the unperturbed field $B_0=2J_0/cr$.

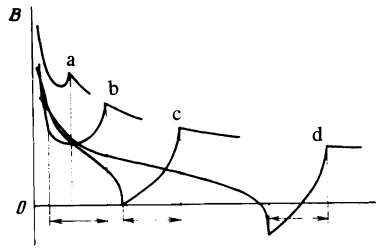

FIG. 4. Profile of magnetic field (12) for four successive instants of time.

At $t<T$, the fact that the current no longer decreases has no effect, and the profile of the field has the smooth form shown in Fig. 4a. At $t>T$, however, at a distance $x_{2f}=c(t-T)$ from the axis, a kink appears on the wave; it can be called a "second front," and behind it, up to the axis, there still remains the so-called "train" of the perturbation, which is a characteristic feature of cylindrical waves (Fig. 4b). At the point $x=x_{2f}=c(t-T)$ of the second front, the field (12) is equal to

$$B(t,x=x_{2f}(t))=\frac{2}{cr_{2f}}\left\{J_0-J_1\left[\left(\frac{2t}{T}\right)^2-1\right]^{1/2}\right\},\quad t>T \tag{13}$$

and inevitably vanishes, after which it becomes negative at

$$t>t^*=\tfrac{1}{2}(\gamma_J^2+1)T,\quad x^*=\tfrac{1}{2}(\gamma_J^2-1)cT.$$

where $\gamma_J=J_0/J_1>1$. The electric field (9) is positive everywhere behind the leading front, since the "$E>B$" situation occurs here in natural fashion. Figure 4 shows the four successive stages of the development of the wave (12).

We consider now the motion of the sheath. For the current (11), the vector potential (9) of the wave is equal to

$$\begin{aligned} &\bar{A}=-\frac{2J_1}{c(s+1)}\tau\left(\operatorname{Arch}\frac{1}{\rho}-\vartheta\right) \quad \text{if} \quad c(t-T)<x<ct,\\ &\bar{A}=-\frac{2J_1}{c(s+1)}\left\{\tau\left[\operatorname{Arch}\frac{1}{\rho}-\vartheta\right]+(1-\tau)\left[\operatorname{Arch}\frac{1}{\rho_T}-(1-\rho_T^2)^{1/2}\right]\right\} \end{aligned} \tag{14}$$

if $0<x<c(t-T)$.

Here

$$\tau=t/T,\quad \rho=x/ct,\quad \vartheta=(1-\rho^2)^{1/2},\quad \rho_T=x/c(t-T).$$

If the sheath was originally at rest at a radius $r=a_1$, corresponding to

$$x=x_1=R(a_1/R)^{s+1/\varkappa(s+1)},$$

then the wave produced on the axis at the instant of time $t=0$ reaches the sheath at the instant $t_1=x_1/c$, which in our interpretation should be regarded as the "true initial instant of time," at which the motion of the sheath begins. Assuming for simplicity that $t_1/T=\gamma_T>1$ and substituting formulas (14) in the relation

$$\bar{A}|_{r=a(t)}=\frac{2J_0}{c}\ln\frac{a(t)}{a_1},$$

it is easy to verify that the equations of motion of the boundary $x=x(t)$ can be written in parametric form

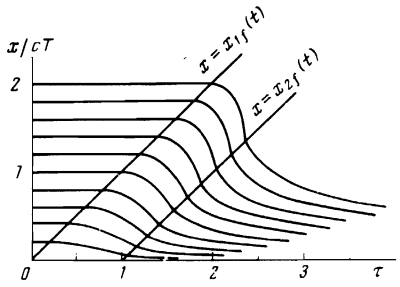

FIG. 5. Family of trajectories (15) of the sheath $x(t)$ for model in which the fictitious current (11) decreases linearly.

$$j(\xi)=\xi\,\mathrm{Arch}\,\xi-(\xi^2-1)^{1/2}=\frac{\gamma_J}{\gamma_T}\eta\ln\eta \quad \text{at} \quad \xi<\xi_2,\ \eta<\eta_2,$$

$$\frac{\gamma_J}{\gamma_T}\eta\ln\eta=\xi\,\mathrm{Arch}\,\xi-(\xi^2-1)^{1/2} \qquad (15)$$

$$-\left(\xi-\frac{\eta}{\gamma_T}\right)\mathrm{Arch}\left(\xi-\frac{\eta}{\gamma_T}\right)+\left[\left(\xi-\frac{\eta}{\gamma_T}\right)^2-1\right]^{1/2} \quad \text{at} \quad \xi>\xi_2,\ \eta>\eta_2.$$

We have introduced here the variables $\xi = ct/x(t) > 1$, $\eta = x_1/x(t) > 1$ and the two parameters $\gamma_J = J_0/J_1 > 1$, $\gamma_T = t_1/T$.

The solutions $x(t)$ of these equations are shown in Fig. 5. The transition values $\xi_2 > 1$ and $\xi_2 > 1$ correspond to the instant $t = t_2 = t_1 + \delta_{12} t\,(\delta_{12} t < T)$ of the transition of the sheath through the second front $x = x_{2f} = c(t - T)$, and are equal to

$$\eta_2=t_1/(t_2-T), \quad \xi_2=t_2/(t_2-T)=1+\eta_2/\gamma_T>\eta_2.$$

Assuming $\xi - 1 \ll 1$ and $\eta - 1 \ll 1$, we obtain from the first equation (15) approximately

$$j(\xi\to 1)=\frac{2\sqrt{2}}{3}(\xi-1)^{3/2}\approx\frac{\gamma_J}{\gamma_T}(\eta-1),$$

$$\xi_2\approx 1+\frac{1}{\gamma_T}>\eta_2=1+\frac{2}{3\gamma_J}\sqrt{\frac{2}{\gamma_T}} \qquad (16)$$

and from this for $t_1 < t < t_2$ we get

$$x(t)\approx x_1\left[1-\frac{2\sqrt{2}}{3}\frac{\gamma_T}{\gamma_J}\left(\frac{t}{t_1}-1\right)^{3/2}\right],$$

$$t_2\approx t_1+T\left(1-\frac{2}{3}\frac{\gamma_T}{\gamma_J}\sqrt{\frac{2}{\gamma_T}}\right). \qquad (17)$$

From the second equation (15) for the asymptotic behavior at $\xi/\eta = t/t_1 \gg 1$ and $\xi > \xi - \eta/\gamma_T \gg 1$ we obtain approximately

$$2\xi\approx\eta^{1/2},\quad \frac{x(t)}{x_1}\approx\left(\frac{t_1}{2t}\right)^{1/(2\gamma_J-1)},\quad \frac{a(t)}{a_1}\approx\left(\frac{t_1}{2t}\right)^{1/(s+1)(2\gamma_J-1)}. \qquad (18)$$

Thus, the radius of the sheath after passing of the second front of the wave decreases quite slowly, and this appears to agree with experiment if it is assumed that the discussed model describes that state of the discharge in deuterium during which neutrons are emitted. The start of the neutron emission in this model should be regarded to be the instant of time $t^* = (\gamma_J^2 + 1)t_1/2\gamma_T$, when the field B_{2f} (13) vanishes.

4. The example considered above, with a linear decrease of the current $J_0(t)$, demonstrates that the "$E > B \sim 0$" situation is inevitable in a wave that moves away from the axis. It is, however, not fully satisfactory, inasmuch as in this example the derivative of the current $J_0(t)$ (11) has discontinuities at $t = 0$ and $t = T$. We therefore investigate another more realistic example of a smooth decrease of the fictitious current:

$$J_0(t)=J_0-J_1\frac{t^2}{t^2+T^2},\quad J_0>J_1, \qquad (19)$$

which makes it possible to calculate the integrals (9) in explicit analytic form. The potential $\tilde{A}$ (9) is in this case

$$\tilde{A}=-\frac{2J_1}{c(s+1)}\int_0^{t-x/c}\frac{t'^2\,dt'}{(t'^2+T^2)[(t-t')^2-(x/c)^2]^{1/2}}=-\frac{2J_1}{c(s+1)}\mathscr{Z}(\rho,\tau), \qquad (20)$$

where we put $\rho = x/ct$, $\vartheta = \sqrt{1-\rho^2}$, $\tau = t/T$ and

$$\mathscr{Z}=\frac{1}{2}\ln\frac{1+\vartheta}{1-\vartheta}-\frac{\sigma_+}{2(\sigma_+^2+\sigma_-^2)}\ln\frac{1+\sigma_+\vartheta}{1-\sigma_+\vartheta}-\frac{\sigma_-\,\mathrm{arctg}\,\sigma_-\vartheta}{\sigma_+^2+\sigma_-^2},$$

$$\sigma_\pm=[(p^2+\tau^2)^{1/2}\pm p]^{1/2},\quad p=\tfrac{1}{2}(1-\vartheta^2\tau^2). \qquad (21)$$

The function $\mathscr{Z}(\rho, \tau)$ is shown in Fig. 6.

Near the front at $\vartheta^2 \ll 1$ we have the expansion

$$\mathscr{Z}=\sum_{k=2}^{\infty}\frac{(1-\rho^2)^{k-1/2}}{2k-1}\left[1-\frac{(\sigma_+^2)^k-(-\sigma_-^2)^k}{\sigma_+^2+\sigma_-^2}\right]\approx\frac{2\tau^2}{15}(1-\rho^2)^{3/2} \qquad (22)$$

and therefore on the front $x = ct$ itself we have

$$E=\partial E/\partial r=B=\partial B/\partial r=0.$$

Near the axis we have approximately

$$\mathscr{Z}|_{\rho\ll 1}=\frac{1}{1+\tau^2}\left[\tau^2\ln\frac{2}{\rho}-\ln(1+\tau^2)^{1/2}-\tau\,\mathrm{arctg}\,\tau+O(\rho^2)\right]. \qquad (23)$$

The motion of the sheath $x = x(t)$ is described now by the equation (starting with the instant $t_1 = x_1/c$)

$$\mathscr{Z}(\rho,\tau)|_{\rho\to x(t)/ct}=\gamma_J\ln\frac{x_1}{x(t)}=\gamma_J\ln\frac{\gamma_T}{\rho\tau} \qquad (24)$$

or in terms of the variables of $\xi = ct/x(t) > 1$, $\eta = x_1/x(t) > 1$ (15) we have

$$\gamma_J\ln\eta=\mathscr{Z}(\rho,\tau) \quad \text{at} \quad \rho\to\frac{1}{\xi},\quad \tau\to\gamma_T\frac{\xi}{\eta},\quad \gamma_T=\frac{t_1}{T}. \qquad (25)$$

Using the first term of the expansion (22), we get for the initial stage of the motion at $\xi = -1 \ll 1$, $\eta - 1 \ll 1$

$$\frac{8\sqrt{2}}{15}(\xi-1)^{5/2}\approx\frac{\gamma_J}{\gamma_T^2}(\eta-1),\quad x(t)=x_1\left[1-\frac{8\sqrt{2}}{15\gamma_J}\gamma_T^2\Big/\left(\frac{t}{t_1}-1\right)^{5/2}\right]. \qquad (26)$$

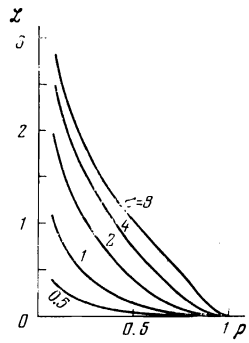

FIG. 6. The function $\mathscr{Z}(\rho, \tau)$ (21) which determines the potential $\tilde{A}$ (20).

Comparison with formula (17) shows that in both cases the initial velocity of the sheath motion is equal to zero, but the initial acceleration $\ddot{a}$ is equal to zero in the case (26) and is infinite in the case (17), this being a definite shortcoming of the above-considered example (11) with the linear decrease of the current $J_0(t)$.

The asymptotic behavior of the sheath as $\tau \to \infty$ coincides in both cases, since formula (23) again leads to expressions (18).

Calculating the derivatives of the function $\mathscr{L}(\rho, \tau)$, we can obtain the electric field

$$\tilde{E} = -\frac{\partial \tilde{A}}{c\,\partial t} = \frac{2J_1}{c^2(s+1)T}\left(\frac{\partial \mathscr{L}}{\partial \tau} - \frac{\rho\,\partial \mathscr{L}}{\tau\,\partial \rho}\right) = \frac{2J_1 F(\rho, \tau)}{c^2(s+1)T} > 0 \qquad (27)$$

and the magnetic field of the wave with the potential $\tilde{A}$ (20):

$$\tilde{B} = -\frac{\partial \tilde{A}}{\partial r} = \frac{2J_1}{cr}\rho\frac{\partial \mathscr{L}}{\partial \rho} = -\frac{2J_1}{cr}G(\rho, \tau) < 0. \qquad (28)$$

If we introduce for brevity the notation $q = (1-\rho^2)p - 1$, then the function F in (27) can be written in the form (see Fig. 7)

$$F = \frac{\tau}{4}\frac{1}{p^2+\tau^2}\left[-2p\vartheta + \left(1 - \frac{2p-4}{(p^2+\tau^2)^{1/2}} + \frac{q-1}{\sigma_+^2}\right)\frac{\sigma_+}{2}\ln\frac{1+\sigma_+\vartheta}{1-\sigma_+\vartheta} - \left(1 + \frac{2p-4}{(p^2+\tau^2)^{1/2}} - \frac{q-1}{\sigma_-^2}\right)\sigma_- \operatorname{arctg}\sigma_-\vartheta\right], \qquad (29)$$

and the function G (28) is equal to (see Fig. 8)

$$G = -\rho\frac{\partial \mathscr{L}}{\partial \rho} = \frac{\rho^2\tau^2}{4(p^2+\tau^2)}\left[2\frac{1-p}{\rho^2}\vartheta + \left(1 - \frac{2p}{(p^2+\tau^2)^{1/2}}\right)\frac{\sigma_+}{2}\ln\frac{1+\sigma_+\vartheta}{1-\sigma_+\vartheta} - \left(1 + \frac{2p}{(p^2+\tau^2)^{1/2}}\right)\sigma_- \operatorname{arctg}\sigma_-\vartheta\right]. \qquad (30)$$

The total magnetic field is equal to (see Fig. 9)

$$B = \frac{2J_0}{cr} + \tilde{B} = \frac{2J_1}{cr}\left[\frac{J_0}{J_1} - G(\rho, \tau)\right] \qquad (31)$$

so that for the "$E > B \approx 0$" situation it is necessary that the condition $G(\rho, \tau) = \gamma_J = J_0/J_1 > 1$ be reached at definite values of ρ^* and τ^*. The experimental value of the parameter γ_J is of the order of unity (~ 1.5), so that G should exceed unity somewhat. It is easily seen, however, that this condition is inevitably reached starting with a certain instant of time τ^*. In fact, if we assume ρ to be fixed and take the limit as $\tau \to \infty$, we obtain

$$p \approx \frac{\rho^2-1}{2}\tau^2, \quad \sigma_- \approx \tau\vartheta, \quad \sigma_+ \approx \frac{1}{\vartheta}\left(1 - \frac{\rho^2}{2\tau^2\vartheta^2} + \ldots\right) \qquad (32)$$

and from formula (30) we get $\lim G(\rho, \tau) = 1/\vartheta$ as $\tau \to \infty$.

The field (28) coincides in this case with the field $\tilde{B}$ (10), which is natural, since the limit $\tau = t/T \to \infty$ corresponds either to $t \to \infty$ or to $T \to 0$, and in the latter case we have an instantaneous interruption of the current (19). Thus, the function $G(\rho, \tau)$, starting with a certain value τ^*, will exceed any prescribed value $\gamma_J > 1$. In the limit as $\tau \to \infty$, the total magnetic field (31) will be negative for ρ in the interval $(1-\gamma_J^{-2})^{1/2} < \rho < 1$.

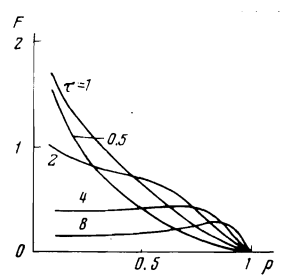

FIG. 7. The function $F(\rho, \tau)$ (29) which determines the field $\tilde{E}$ (27).

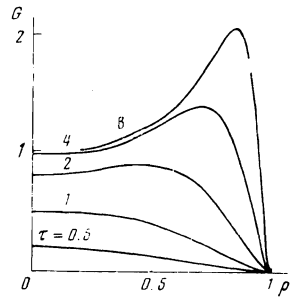

FIG. 8. The function $G(\rho, \tau)$ (30) which determines the field $\tilde{B}$ (28).

We consider next the ratio of the fields (28) and (31):

$$\frac{E}{B} = \frac{r}{cT(s+1)}\frac{F(\rho, \tau)}{\gamma_J - G(\rho, \tau)} = \theta_\varkappa \frac{F(\rho, \tau)}{\gamma_J - G(\rho, \tau)}(\rho\tau)^{1/(s+1)}. \qquad (33)$$

Here $\theta_\varkappa = \varkappa[R/(s+1)\varkappa cT]^{s/(s+1)}$ is a small coefficient. For example, at $\varkappa = 10^{-4}$, $R = 50$ cm, $T = 100$ nsec, and $s = \frac{3}{2}$ we have $\theta_\varkappa \approx 10^{-3}$. Inasmuch as $E/B = \dot{a}/c$ on the boundary of the pinch, it is precisely the smallness of the coefficient $\theta_\varkappa$ which ensures the relative slowness of the motion of the sheath with velocity $\dot{a} \sim c\theta_\varkappa \sim 3 \cdot 10^7$ cm/sec, as is observed in experiment.

Inasmuch as the remaining factors in (33) are of the order of unity (at $\rho \sim 1$ and $\tau \sim 1$), the "$E > B \approx 0$" situation, which is necessary for the particle acceleration, is possible only in an extremely narrow gap with dimensions of the order of

$$|\rho - \rho^*| \sim [\theta_\varkappa/(\partial^2 G/\partial\rho^2)_{\rho^*}]^{1/2}$$

in the immediate vicinity of the point ρ^*, where the denominator (33) vanishes at $G = \gamma_J$. It is necessary here that the sheath be able to jump through the dangerous place of the wave before the field B (31) vanishes. Only in this case the "$E > B \approx 0$" situation will be produced outside the sheath, which at that instant should already

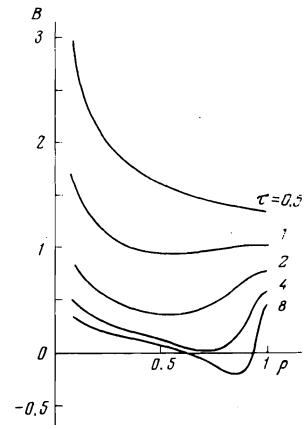

FIG. 9. Profile of the total magnetic field (31) for the parameter $\gamma_J = \frac{7}{5}$.

be closer to the axis and decelerate approximately in accordance with formulas (18). These conditions can be insured if, given the parameter $\gamma_J > 1$ in the equation of motion of the sheath (24), the second parameter $\gamma_T = t_1/T$ is smaller than a certain critical value γ_T^{cr}.

This critical value is obtained if it assumed that the sheath at the instant τ^* is located at the point ρ^*, and γ_T^{cr} is determined by the relation

$$\mathcal{L}(\rho^*, \tau^*) = \gamma_J \ln(\gamma_T^{cr}/\rho^*\tau^*), \quad (34)$$

whereas the position of the sheath at the instant τ^* is determined by Eq. (24):

$$\mathcal{L}(\rho(\tau^*), \tau^*) = \gamma_J \ln[\gamma_T/\tau^*\rho(\tau^*)].$$

Recognizing that

$$G(\rho, \tau^*) = -\rho\partial\mathcal{L}/\partial\rho < G^{max}(\rho, \tau^*) = \gamma_J, \quad (35)$$

and subtracting relation (34) from (35), we obtain

$$\int_{\rho(\tau^*)}^{\rho^*} [\gamma_J - G(\rho, \tau^*)] \frac{d\rho}{\rho} = \gamma_J \ln \frac{\gamma_T^{cr}}{\gamma_T} > 0. \quad (36)$$

We see therefore that for $\rho(\tau^*) < \rho^*$ it is necessary to satisfy the condition $\gamma_T < \gamma_T^{cr}$, that is, the sheath must begin its motion early enough to be able to jump through the dangerous region of the wave. The values of γ_T^{cr} are listed in the table. It is seen from the table that, with good accuracy, $\gamma_T^{cr} = \tau^* - 0.4$. At a given $\gamma_J > 1$, only values $\gamma_T < \gamma_T^{cr}$ are allowed.

5. For comparison with experiment, we note that the theory contains a rather large number of parameters, the choice of which can lead to close agreement. In Fig. 10, taken from the paper of Filippov *et al.*,[11] is shown the time variation of the radius of the constriction $a(t)$ in the narrowest place of the plasma focus, and also the neutron and x-ray emission. The experimental time t^{exp} is arbitrarily reckoned from the start of the x-ray emission. In accordance with our model, the decreasing part of the $a(t)$ curve should agree with the asymptotic formula (18)

$$a(t)/a_1 \approx (t_1/2t)^k, \quad k = 1/(s+1)(\gamma_J - 1), \quad (37)$$

where the instant of the maximum $a_1 = 11.5$ mm is assumed in the theory to be the instant of time t_1. If it is assumed that $t_1 \ll 100$ nsec, then, choosing on Fig. 10 two points, $a(t^{exp} = 200\ \text{nsec}) = 2.3$ mm and $a(t^{exp} = 300) = 1.75$ mm, we obtain for their ratio, in accordance with (37), the value $2.3/1.75 = 2^k$, therefore $k \approx 0.4$, which corresponds at $s = \frac{3}{2}$ to the choice $\gamma_J = 2$ and $t_1 = 4$

Characteristics of the maximum of the function $G(\rho, \tau)$ (30).

$\tau = \tau^*$	Maximum G	ρ^*	$\mathcal{L}(\rho^*, \tau^*)$	$\rho^*\tau^* = \frac{x^*}{cT}$	γ_T^{cr}	$F(\rho^*, \tau^*)$
< 2	<1	—	—	—	—	—
3	1.165	0.63	0.37	1.89	2.6	0.525
4	1.39	0.725	0.3	2.9	3.6	0.425
5	1.58	0.77	0.27	3.85	4.56	0.375
6	1.75	0.81	0.24	4.86	5.55	0.335
7	1.91	0.835	0.23	5.85	6.55	0.31
8	2.045	0.855	0.21	6.84	7.6	0.285
9	2.18	0.87	0.2	7.83	8.6	0.265
10	2.31	0.885	0.19	8.85	9.6	0.25
11	2.425	0.89	0.186	9.79	10.6	0.24
12	2.504	0.9	0.178	10.8	11.6	0.23

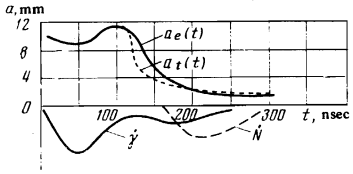

FIG. 10. Experimental and theoretical (dashed) time dependences of the sheath radius $a(t)$, and also of the neutron and x-ray emissions (from[10]).

nsec. If it is assumed that the maximum $a_1 = 11.5$ occurs at $t^{exp} = 110$ nsec, and the instant of the start of the neutron emission and the second burst of the x-rays occur at the instant $t^{exp} = 150$ nsec, then, in accordance with the table, we find that at $\gamma_J = 2$ the situation $B = 0$ is reached at the instant $\tau^* = 8 = (t_1 + 40)/T$, from which we obtain at $t_1 = 4$ nsec the value $T = 5.5$ nsec, meaning $\gamma_T = t_1/T \approx 0.75$. By choosing $\gamma_J = 2$ and $\gamma_T = \frac{3}{4}$, we can obtain from the equation of motion of the sheath $\mathcal{L}(\rho, \tau) = 2\ln(0.75/\rho\tau)$ a more accurate theoretical relation for $a(t)$ (shown dashed in Fig. 10) and again compared with the experimental curve.

At small $\rho \ll 1$ we can use the asymptotic formula (23), from which we get

$$\frac{a(t)}{a_1} \approx \left[\frac{3}{8\tau}(1+\tau^2)^{1/2\tau^2} \exp\left(\frac{1}{\tau}\operatorname{arctg}\tau\right)\right]^{1/(s+1)(1+2\tau^{-2})}. \quad (38)$$

This yields, for example, $a = 7.5$ mm at $\tau = 3$ and $t^{exp} = 122.5$ nsec, so that within 12 nsec $a(t)$ decreases by approximately 4 mm, moving with a speed $\sim 3 \cdot 10^7$ cm/sec. At t close to t_1, formula (26) is valid, from which we obtain

$$\frac{a(t)}{a_1} \approx \exp\left[-\left(\frac{t-t_1}{t_{eff}}\right)^{3/s}\right], \quad t_{eff} = t_1\left[\frac{15}{8\sqrt{2}}\frac{\gamma_J(s+1)}{\gamma_T^2}\right]^{3/s} \approx 11\ \text{nsec}. \quad (39)$$

Formulas (38) and (39) are in qualitative agreement with the data of Fig. 10. The relation $ct_1 = x_1 = 120$ cm $= R(a_1/R)^{s+1}/\varkappa(s+1)$ at $a_1 \approx 1$ cm and $s = \frac{3}{2}$ is also approximately satisfied, if it is assumed that $\varkappa \approx 10^4$ and $R = R_{eff} = 10$ cm.

The point where the particles begin to be accelerated is determined accordance with the table by the relation

$$\frac{a(t)}{a_1}\Big|_{\tau^*=8,\ \rho^*=0.855} = \left(\frac{x}{x_1}\right)^{1/(s+1)} = \left(\frac{\rho^*\tau^*}{\gamma_T}\right)^{3/s} \approx 2.4, \quad (40)$$

that is, it is approximately twice as far as the initial radius of the sheath. From Fig. 10 and from the table we can find that the electric field is in this case equal to (we assume $J_0 = 10^6$ A)

$$E^* = \frac{2J_1}{c^2T(s+1)}F(\rho^*, \tau^*) \approx 20\ \text{kV/cm}, \quad (41)$$

so that, for example, the particles can acquire an energy 100 keV by covering a path of approximately 5 cm.

This value still seems insufficient to explain the observed energies of the accelerated particles (~300 keV), but it must be noted that the considered model is only a rough approximation of reality. It does not take into account, in particular, the dependence of the fields on the coordinate z, an important factor in the case of

necks (see[6]). In addition, the relation $c_A(r) = (R/r)^s c_A^w$ assumed above for the Alfven velocity is valid only on the wave front, but behind the front the magnetic field decreases with time, so that actually it would be necessary to consider nonlinear wave equations, which can be solved only numerically.

The authors are quite grateful to M. A. Leontovich and S. Yu. Luk'yanov for discussions, and also to N. V. Filippov, M. I. Stepanenko, and T. I. Filippova for supplying valuable information on the experimental data.

[1)]A similar mechanism was considered in[7].

[1]L. A. Artsimovich, Upravlyaemye termoyadernye reaktsii (Controlled Thermonuclear Reactions), Fizmatgiz, 1961, Chap. V.
[2]L. A. Artsimovich, A. M. Andrianov, E. I. Dobrokhotov, S. Yu. Luk'yanov, I. M. Podgornyĭ, V. N. Sinitsyn, and N. V. Filippov At. Énerg. 3, 76 (1956).
[3]V. I. Agafonov, I. F. Belyaeva, V. V. Vikhrev, V. D. Ivanov, M. I. Moiseeva, E. B. Svirskiĭ, N. V. Filippov, and T. I. Filippova, Preprint IAÉ-2017, 1970.
[4]K. D. Ware *et al.*, Bull. Am. Phys. Soc. **18**, 1364 (1973).
[5]B. A. Trubnikov, in: Fizika plazmy i problema UTR (Plasma Physics and the Problem of Controlled Thermonuclear Reactions) 1, Izd. Akad. Nauk SSSR, 1958, p. 289.
[6]V. A. Trubnikov, *ibid.*, 4, p. 87.
[7]J. Fukai and E. J. Clothianx, Phys. Rev. Lett. **34**, 863 (1975).
[8]V. A. Gribkov, Dissertation, 1973.
[9]A. Bernard, A. Condeville, A. Jolas, J. Launspach, and J. de Marcureau, Phys. Fluids **18**, 180 (1975).
[10]V. V. Aleksandrov, N. G. Koval'skiĭ, S. Yu. Luk'yanov, V. A. Rantsev-Kartinov, and M. M. Stepanenko, Zh. Eksp. Fiz. Teor. **64**, 1222 (1973) Sov. Phys.-JETP **37**, 622 (1973).
[11]N. V. Filippov, V. D. Ivanov, M. P. Moiseeva, M. M. Stepanenko, and N. K. Sukhareva, (Analysis of the Geometry, Dynamics, and Magnetic Structure of a Plasma Focus by the Laser Interferometry Method, Paper at 5th Conf. on Controlled Fusion and Plasma Physics, Tokyo, 1974.

Translated by J. G. Adashko

Electrical properties and dependence of the *s-f* exchange integral on atomic volume of single crystals of gadolinium-dysprosium alloys

S. A. Nikitin, S. S. Slobodchikov, and O. D. Chistyakov

Moscow State University
and Metallurgy Institute, USSR Academy of Sciences
(Submitted December 17, 1974; resubmitted July 23, 1975)
Zh. Eksp. Teor. Fiz. **70**, 104–114 (January 1976)

An investigation was made of the electrical resistivity of gadolinium-dysprosium alloy single crystals as a function of temperature, magnetic field, and hydrostatic pressure. The temperature dependences of the electrical resistivity had kinks and maxima at the Curie and Néel points and these singularities depended strongly on whether the direction of current flow was parallel to the hexagonal axis or in the basal plane. The magnetic component of the resistivity was determined. The theory of indirect exchange and experimental information on the electrical resistivity and its pressure dependence were used to calculate the *s-f* exchange integral and the effective mass of conduction electrons, and the dependences of these quantities on the atomic volume.

PACS numbers: 72.15.Gd, 72.15.Eb, 71.70.Gm

Rare-earth metals and alloys are characterized by record values of the resistivity at room temperature due to the very large magnetic component of the resistivity at temperatures exceeding the magnetic ordering point. The scattering of conduction electrons by a system of spins which is not in an ideal magnetic order clearly increases with the spin of the scattering atoms (other conditions being constant). The spin is largest for rare-earth metals and particularly for gadolinium, for which we have $S=\frac{7}{2}$. Therefore, anomalies due to the magnetic component of the resistivity are strongest for rare-earth metals and alloys and this makes it easy to study them and compare the experimental and theoretical results. The electrical resistivity of rare-earth metals and alloys is also of interest because the greatest success in the description of electrical properties of transition metals, on the basis of the indirect exchange theory, has been achieved for these materials.[1–3] The localization of the $4f$ electrons makes it easier to develop a theory which gives correct values of the exchange parameters (at least in respect of the order of magnitude) and describes, in agreement with experiment, the dependence of the paramagnetic Curie point and electrical resistivity on the atomic constants of rare-earth ions.

The electrical resistivity of pure rare-earth metals has been investigated using polycrystalline and single-crystal samples.[4–8] However, studies of the electrical properties of rare-earth alloys have only been carried out on polycrystalline samples,[9–11,20] which is insufficient in view of the strong anisotropy of the properties along the hexagonal axis and in the basal plane. We shall report the results obtained for gadolinium–dys-